Glycolysis-stratified coordination of fatty acid and glutamine metabolism in pancreatic ductal Adenocarcinoma

Salma Fareed[1,2]

[1]The Winter Lab, Case Comprehensive Cancer Center, Cleveland, OH 44106
[2]Department of Sciences, Hathaway Brown School, Shaker Heights, OH 44122

Abstract

Pancreatic ductal adenocarcinoma (PDAC) relies heavily on rewired glutamine (GLN) and fatty-acid (FA) metabolism, but whether these programs coordinate in a glycolysis-dependent manner and across FA chain-length or functional families remains unclear. RNA-seq and clinical data from a multi-institutional cohort (n = 172) were analyzed; FA and GLN pathway activities were inferred by single-sample gene set variation analysis (ssGSEA), tumors were stratified by glycolysis state, and FA–GLN associations were evaluated at pathway, enzyme-class (medium, long, and very-long-chain; VLCFA ≥ C20), and family levels using correlation, Fisher-z meta-analysis, and bootstrap resampling. FA–GLN coordination varied with glycolysis: membrane-focused families (glycerophospholipids, sphingolipids) coupled most strongly to GLN in low-glycolysis tumors; coupling shifted toward very-long-chain FA enzymes in medium-glycolysis tumors; and weakened in high-glycolysis tumors. Family-level contrasts confirmed weaker glycerophospholipid and sphingolipid coupling in high versus low glycolysis. A complementary metabolite-inference analysis identified three metabolic phenotypes that preserved these glycolysis-stratified FA–GLN relationships, supporting a broader coordinated metabolic structure. Survival analyses suggested state and chain length-specific trends. These results delineate a glycolysis-stratified map of FA–GLN coordination in PDAC and nominate testable metabolic vulnerabilities with potential therapeutic and dietary relevance.

Introduction

Pancreatic ductal adenocarcinoma (PDAC) is the most common form of pancreatic cancer and remains among the most lethal solid tumors. Despite progress in detection and therapy, the five-year survival rate

remains below 12%, and incidence is projected to rise in the coming decades [1,2]. Most patients present with advanced or metastatic disease, and the limited benefit of current chemotherapies underscores the need for alternative therapeutic strategies [2]. In addition to genetic alterations, PDAC progression is shaped by metabolic adaptations that enable tumor cells to persist and proliferate in a hypoxic, nutrient-poor microenvironment [3,4]. Altered metabolism is recognized as a defining hallmark of malignancy, and PDAC is a typical example of metabolic plasticity [3,5]. The PDAC microenvironment is nutrient-limited, driving changes in nutrient use and energy pathways and fostering mechanisms such as extracellular protein scavenging [6]. In PDAC, glycolysis remains high despite oxygen availability, generating biosynthetic building blocks and redirecting metabolic dependencies [7]. Molecular subtyping indicates that glycolysis-high tumors tend to be more aggressive and linked to poorer clinical outcomes [8].

Glutamine (GLN) metabolism is central to PDAC biology. GLN provides carbon and nitrogen for nucleotide synthesis, sustains redox balance via glutathione, and replenishes the tricarboxylic acid (TCA) cycle through anaplerosis [9]. Oncogenic KRAS reprograms GLN utilization through non-canonical routes that support tumor growth [10]. Inhibition of GLN metabolism slows PDAC proliferation, but compensatory nutrient routes are frequently engaged [9,11]. Pharmacologic blockade with 6-diazo-5-oxo-L-norleucine (DON) has been shown to trigger a metabolic crisis in PDAC models, yet rapid adaptive responses were observed [12]. Stromal interactions also provide alternative substrates (e.g., alanine), complicating therapeutic targeting [13]. Direct metabolomic measurements on resected human PDAC tissue have demonstrated reduced glutamine relative to paired benign pancreas, underscoring nutrient limitation in the tumor microenvironment [6], emphasizing the importance of nutrient context.

Fatty acid (FA) metabolism likewise contributes substantially to PDAC. De novo lipogenesis and FA uptake furnish membrane components, signaling lipids, and energy reserves [14]. Enzymes that elongate and desaturate fatty acids (e.g., ELOVL, FADS, SCD) enable lipid remodeling and can promote oncogenic signaling [15]. PDAC cells also draw on exogenous lipids and alternative carbon sources such as acetate, reinforcing metabolic flexibility [16]. Distinct FA subclasses; medium-chain (MCFA), long-

chain (LCFA), and very-long-chain fatty acids (VLCFA), likely exert different effects on tumor behavior, yet systematic, patient-based evaluation has been limited [17].

The interplay between FA and GLN metabolism in PDAC has been highlighted experimentally. Inhibition of GLN metabolism sensitizes tumors to ketogenic-diet conditions, revealing vulnerabilities when glucose and lipid pathways are simultaneously perturbed [18]. Additional work supports coordination between FA programs and GLN pathways and motivates combined therapeutic strategies targeting both axes [15,19]. However, FA metabolism is often treated as a single pathway, with limited attention to chain-length or family-specific diversity. Moreover, it remains unclear whether FA–GLN coordination is a general feature of PDAC or conditional on glycolytic activity. This gap is particularly relevant because ketogenic diets alter circulating FA chain-length distributions and patient tumors vary widely in glycolytic state [18].

To address these questions, transcriptomic and clinical data from a multi-institutional PDAC cohort (n = 172) were analyzed. FA–GLN associations were evaluated across glycolytic strata, and chain-length–specific FA families were examined for prognostic and metabolic differences. A two-tier analytic framework was applied, combining broad profiling of curated FA pathways with targeted interrogation of MCFA, LCFA, and VLCFA families. Enzyme-class (chain-length) and family-level (functional) analyses were used to capture functional diversity, and associations with GLN were quantified using Elastic Net regression with bootstrap resampling. To my knowledge, this represents the first patient-based study to link FA–GLN coupling explicitly to glycolytic stratification in PDAC, delineating context-specific vulnerabilities with potential therapeutic and dietary relevance.

Methods

Data source and preprocessing

RNA-seq and clinical data from the AACR Project GENIE PDAC cohort (n = 172) were analyzed [20]. Clinical variables included age, sex, stage, and tumor mutational burden (TMB). Gene-level expression counts were normalized to log□ transcripts per million (TPM). Quality control included verification of

identifiers, consistency of clinical annotations, and exclusion of samples failing RNA-seq metrics (e.g., low library complexity, missing covariates). Genes with low expression (counts per million < 1 in > 80% of samples) were excluded. One sample had complete expression data but lacked clinical annotations; therefore, analyses requiring clinical covariates used n = 172, while metabolite-inference analyses used n= 173. Pathway curation FA and GLN pathways were curated from KEGG and Reactome [21,22], including biosynthesis and degradation processes. Pathways were grouped into MCFA, LCFA, and VLCFA classes to capture chain length–specific biology [14,17]. In addition to chain-length classes, pathways and enzymes were grouped into functional FA families (e.g., sphingolipids, glycerophospholipids, triglycerides, lipid transport, FA biosynthesis/elongation, FA oxidation, FAO carnitine shuttle, lipid regulatory, and unsaturated FA) using KEGG/Reactome and WikiPathways annotations [23]; families could span chain-length classes. Glycolysis stratification used the MSigDB Hallmark Glycolysis gene set [24]. The pathway-to-family mapping is provided in Supplementary Table S2.

Pathway activity scoring

Pathway activity scores were computed with single-sample gene set variation analysis (ssGSEA) using the GSVA R package [25]. Patients were stratified into low, medium, and high glycolysis groups by tertiles of the Hallmark Glycolysis score. Pathway scores were z-standardized so that effects were expressed per one standard deviation (1 SD) increase.

FA–GLN correlations stratified by glycolysis state

Spearman correlations were calculated between FA and GLN pathway activity within each glycolysis stratum. Multiple testing correction used the Benjamini-Hochberg false discovery rate (FDR) procedure with a threshold of FDR ≤ 0.20 [26].

FA pathway activity and tumor stage

Associations between FA activity and AJCC stage were evaluated with linear regression adjusted for age, sex, and TMB. Regression coefficients (β_stage), p-values, FDR-adjusted q-values, and R^2 were reported.

Enzyme-class correlations with glutamine

Enzyme activity was defined as the z-score of expression for genes encoding FA metabolic enzymes. Enzyme–GLN correlations were estimated within glycolysis strata. Correlations were aggregated into MCFA, LCFA, and VLCFA classes using random-effects meta-analysis with inverse-variance weighting of Fisher's z -transformed values; pooled estimates were back-transformed to correlation coefficients. Bootstrap resampling (B = 5,000) was used to quantify uncertainty.

Family-level comparisons

Enzyme-level correlations were combined within families using Fisher's z transformation to obtain pooled meta-correlations. Differences between glycolysis states (Δr_meta) were assessed with bootstrap resampling (B = 5,000). Two-sided p-values were derived from bootstrap distributions and FDR-adjusted across families.

Survival analysis stratified by glycolysis

Overall survival was analyzed using Cox proportional hazards models adjusted for age, sex, and stage; hazard ratios (HRs) and 95% confidence intervals (CIs) were reported [27].

- Enzyme-class level: enzyme-specific log(HR) estimates were pooled within MCFA, LCFA, and VLCFA classes using random-effects meta-analysis.
- Family level: ssGSEA-derived FA family scores were evaluated within each glycolysis stratum using Cox models.

Predictive modeling

Elastic Net regression tested whether FA activity predicted GLN activity within glycolysis strata. Models included age, sex, stage, and TMB as covariates. Performance was evaluated using R^2. Permutation testing (1,000 permutations) generated null R^2 distributions for comparison [28,29].

Supplementary Metabolite Inference and Metabolic-State Assignment

A curated metabolite–gene mapping was assembled to infer activity for 13 metabolites relevant to glutamine metabolism (GLN, GLU, αKG), tricarboxylic acid (TCA) cycle intermediates (CITRATE,SUCCINATE, FUMARATE, MALATE), pyruvate–lactate exchange (PYRUVATE, LACTATE), fatty-acid oxidation (short/medium and long chain acyl-carnitines), very long chain fatty acid elongation (VLCFA_ELONG), and cellular redox buffering (GSH/GSSG). Enzymatic reactions were annotated as production or consumption steps, and associated genes were assigned weights of +1 or –1 accordingly.

For each metabolite, a weighted mean expression value was calculated across all mapped genes. All metabolite scores were then z-normalized across samples to produce a 13 × 173 activity matrix. Principal component analysis followed by k = 3 clustering was applied to the normalized metabolite activity matrix to define three metabolite-based tumor states (Supplementary Fig. S3 and Supplementary Fig. S4). These states were annotated based on characteristic metabolic signatures and were designated as the Oxidative GLN-Driven State (GLN_TCA_REDOX_HIGH), the Hybrid FAO–TCA State (TCA_GLYCOLYTIC_FAO_HIGH), and the Glycolytic FAO-Low State (FAO_LOW). Associations between the three metabolite-defined states and the glycolysis strata (Low, Medium, High) were evaluated using the chi square test of independence, and effect size was quantified using Cramér's V. Differences in individual metabolite activities across the three metabolite-defined states were evaluated using one-way ANOVA and the Kruskal–Wallis test. All analyses were performed only when ≥2 samples per state were available, and statistical significance was determined using Benjamini–Hochberg FDR correction. Significant differences (FDR < 0.05) were detected for all 13 metabolites in both tests, confirming that each metabolite-defined state represented a distinct metabolic phenotype. Complete

statistical outputs for metabolite activity comparisons are provided in Supplementary Table S4, and the metabolite–gene mapping and metabolic-state labels are provided in Supplementary Table S5 and Supplementary Data S5, respectively.

Implementation

Analyses were performed in R (v4.3) and Python (v3.12). ssGSEA was run with GSVA [25]; glycolysis scores used the MSigDB Hallmark Glycolysis set [24]. In Python, data handling used NumPy and pandas [30,31]; Elastic Net and permutation tests were implemented with scikit-learn [32]; figures were generated with Matplotlib [33].

Prespecified statistical thresholds differed by analysis type: FA–GLN pathway correlations used an FDR ≤ 0.20; tumor-stage associations used FDR ≤ 0.25 due to smaller effect sizes; analyses using q-values (family-level Δr comparisons and metabolite-inference tests) used FDR < 0.05; and survival analyses report nominal p-values without FDR correction.

Results

FA–GLN correlations stratified by glycolysis state

Spearman correlations between fatty acid (FA) pathway activity and glutamine (GLN) activity differed by glycolysis state (Fig 1, Table 1). In glycolysis-low tumors, sphingolipid pathways showed the strongest positive correlations with GLN, including Sphingolipid pathway (ρ = 0.44, FDR = 0.063), Sphingolipid metabolism overview (ρ = 0.39, FDR = 0.104), Sphingolipid de novo biosynthesis (ρ = 0.35, FDR = 0.104), and Sphingolipid metabolism integrated pathway (ρ = 0.35, FDR = 0.104). Glycerophospholipid biosynthesis also correlated positively (ρ = 0.35, FDR = 0.104). In glycolysis-medium tumors, the strongest correlations were observed for aminoacyl-tRNA pathways; tRNA aminoacylation (ρ = 0.46, FDR = 0.024), Mitochondrial tRNA aminoacylation (ρ = 0.45, FDR = 0.024), and Aminoacyl-tRNA biosynthesis (ρ = 0.42, FDR = 0.033). Lipid-associated pathways, including Peroxisomal lipid

metabolism (ρ = 0.38, FDR = 0.078) and Mitochondrial fatty acid oxidation disorders (ρ = 0.36, FDR = 0.078), were also positively correlated. In glycolysis-high tumors, no FA pathways met the prespecified FDR ≤ 0.20 threshold.

Elastic-Net regression did not outperform permutation-derived null distributions, indicating that FA pathways, while associated with GLN, do not provide strong predictive power for GLN activity. These aminoacyl-tRNA correlations are interpreted as reflecting general GLN-dependent biosynthetic demand rather than fatty acid–specific metabolic regulation.

Fig 1. Volcano plots of FA–GLN correlations by glycolysis state.

Spearman correlation coefficients (ρ) are shown on the x-axis and −log□ □(FDR) on the y-axis. Points are colored by glycolysis state (Low = red, Medium = blue, High = green). Dashed lines indicate |ρ| = 0.20 and FDR ≤ 0.20 (significance). In Low glycolysis, several sphingolipid modules reached significance; in Medium glycolysis, aminoacyl-tRNA pathways reached significance. No pathways met FDR ≤ 0.20 in High glycolysis; near-threshold trends are displayed for context. **Abbreviations**: FA, fatty acid; GLN, glutamine; FDR, false discovery rate.

Table 1. Top fatty acid pathways correlated with glutamine activity by glycolytic state.

Pathway (source)	Glycolysis state	Spearman ρ	FDR (q)
Sphingolipid pathway (WikiPathways)	Low	0.44	0.063
Sphingolipid metabolism overview (WikiPathways)	Low	0.39	0.104
Sphingolipid metabolism (KEGG)	Low	0.38	0.104
Metabolism of sphingolipids in ER and Golgi apparatus (Reactome)	Low	0.37	0.104
Sphingolipid de novo biosynthesis (Reactome)	Low	0.35	0.104
Sphingolipid metabolism—integrated pathway (WikiPathways)	Low	0.35	0.104
Gargalovic response to oxidized phospholipids (MSigDB CGP)	Low	0.35	0.104

Pathway (source)	Glycolysis state	Spearman ρ	FDR (q)
Glycerophospholipid biosynthetic pathway (Reactome/WikiPathways)	Low	0.35	0.104
Sphingolipid metabolism (Reactome)	Low	0.34	0.111
Gargalovic response to oxidized phospholipids (MSigDB CGP)	Low	0.33	0.123
tRNA aminoacylation (Reactome)	Medium	0.46	0.024
Mitochondrial tRNA aminoacylation (Reactome)	Medium	0.45	0.024
Aminoacyl-tRNA biosynthesis (KEGG)	Medium	0.42	0.033
Peroxisomal lipid metabolism (Reactome)	Medium	0.38	0.078
Mitochondrial fatty acid oxidation disorders (Reactome)	Medium	0.36	0.078

Abbreviations: FDR, false discovery rate; ER, endoplasmic reticulum; MSigDB CGP, Molecular Signatures Database-chemical/genetic perturbations collection.

FA pathway activity and tumor stage

Linear regression models tested associations between FA pathway activity and AJCC stage (Fig 2, Table 2). Pathway activity generally decreased with advancing stage. The most negative coefficients were observed for Elevated circulating long-chain fatty acid concentrations (β_stage = –1.23, p = 0.183, FDR = 0.842), Very-long-chain fatty acid accumulation (β_stage = –0.92, p = 0.106, FDR = 0.981), Medium chain fatty-acyl-CoA metabolic process (β_stage = –0.86, p = 0.234, FDR = 0.697), and Very-long-chain fatty acid CoA ligase activity (β_stage = –0.74, p = 0.171, FDR = 0.981). None remained significant after multiple-testing correction.

Fig 2. Associations between FA pathway activity and tumor stage.

Multivariable linear regression coefficients for tumor stage (β_stage) are shown for FA pathways, adjusted for age, sex, and tumor mutational burden. Colors denote FA families (MCFA=red, LCFA=blue, VLCFA=green). The vertical dashed line marks no association (β_stage = 0). Pathways with the largest absolute β_stage within each family are highlighted. No pathway met FDR ≤ 0.25. **Abbreviations**:

MCFA, medium chain fatty acid; LCFA, long chain fatty acid; VLCFA, very long chain fatty acid; TMB, tumor mutational burden.

Table 2. Associations between fatty acid pathway activity and tumor stage in PDAC.

Regression coefficients for tumor stage (β_stage) were estimated from multivariable linear models of pathway activity, adjusted for age, sex, and tumor mutational burden (TMB). Pathways with |β_stage| ≥ 0.70 are shown (n = 166 patients with complete data). No pathway met the prespecified significance threshold of FDR ≤ 0.25.

FA family	Pathway	β_stage	P value	FDR (q)	R^2
LCFA	Elevated circulating long-chain fatty acid concentrations	–1.23	0.183	0.842	0.015
LCFA	Long chain fatty acid–CoA ligase activity	–0.72	0.116	0.842	0.024
MCFA	Medium chain fatty-acyl-CoA metabolic process	–0.86	0.234	0.697	0.010
VLCFA	Very long chain fatty acid accumulation	–0.92	0.106	0.981	0.018
VLCFA	Very long chain fatty acid–CoA ligase activity	–0.74	0.171	0.981	0.016

Abbreviations*:* FA, fatty acid; LCFA, long chain FA; MCFA, medium chain FA; VLCFA, very long chain FA; TMB, tumor mutational burden; FDR, false discovery rate.

Notes: AJCC stage was treated as an ordinal variable (I–IV); β_stage reflects the change in pathway activity per one-stage increase (negative values indicate lower activity at higher stage).

Enzyme-class correlations with glutamine

Class-level meta correlations between FA enzyme length classes and GLN activity were estimated by pooling enzyme-specific Spearman correlations (Fisher's z random-effects) and are shown in Fig 3 and Table 3. In glycolysis-medium tumors, very-long-chain fatty acid (VLCFA) enzymes showed the strongest positive correlation with GLN (r =0.23, 95% CI 0.09–0.34), followed by medium-chain fatty acid (MCFA) enzymes (r = 0.17, 95% CI 0.06–0.28). In glycolysis-low tumors, MCFA enzymes were weakly positive (r = 0.09, 95% CI –0.02 to 0.20), whereas VLCFA enzymes were near zero (r = 0.04,

95% CI –0.15 to 0.15). LCFA enzymes were weakly positive across states (r = 0.04-0.06). In glycolysis-high tumors, MCFA enzymes trended slightly negative (r = –0.05, 95% CI –0.20 to 0.10).

Fig 3. Association of FA enzyme length classes with GLN correlations across glycolysis states. Fisher's meta-correlation coefficients (r) between enzyme-level FA activity and GLN activity are shown for MCFA, LCFA, and VLCFA classes within each glycolysis state (Low = blue, Medium = orange, High = red). Error bars indicate 95% confidence intervals from bootstrap resampling (B = 5,000). The vertical dashed line marks no association (r = 0). Abbreviations: MCFA, medium chain fatty acid; LCFA, long chain fatty acid; VLCFA, very long chain fatty acid.

Table 3. Meta-correlation of fatty acid enzyme classes with glutamine activity by glycolysis state. Fisher's meta-correlation coefficients (r) were calculated within each glycolysis state for medium chain (MCFA), long chain (LCFA), and very long chain (VLCFA) enzyme classes. Values are shown with 95% confidence intervals from bootstrap resampling (B = 5,000). No associations met the prespecified FDR ≤ 0.25 threshold.

FA class	Glycolysis state	Meta-correlation (r)	95% CI lower	95% CI upper
MCFA	Low	0.09	−0.02	0.20
MCFA	Medium	0.17	0.06	0.28
MCFA	High	−0.05	−0.20	0.10
LCFA	Low	0.06	−0.02	0.13
LCFA	Medium	0.04	−0.03	0.13
LCFA	High	0.05	−0.03	0.14
VLCFA	Low	0.04	−0.15	0.15
VLCFA	Medium	0.23	0.09	0.34
VLCFA	High	0.15	−0.11	0.29

Abbreviations: MCFA, medium-chain fatty acid; LCFA, long-chain fatty acid; VLCFA, very-long-chain fatty acid; CI, confidence interval.

Family-level comparisons

Family-level FA–GLN associations (Fig 4, Table 4; Supplementary Table S2 for family mappings) showed significant decreases in high versus low-glycolysis tumors for glycerophospholipids (Δr_meta = –0.06, p = 0.0041, q = 0.021) and sphingolipids (Δr_meta = –0.12, p = 0.0019, q = 0.019). Other families (FA biosynthesis/elongation, FAO β-oxidation, lipid transport, triglycerides, unsaturated FA, FAO carnitine shuttle, lipid regulatory) did not pass q < 0.05.

Fig 4. Family-level shifts in FA–GLN coupling by glycolysis state.

(A) Scatterplot comparing family-level meta-correlations (r) in High versus Low glycolysis tumors; each point is an FA family. Families with significant differences (Δr, High–Low) at FDR q < 0.05 are highlighted. (B) Bar plot of Δr (High–Low) with corresponding p- and q-values; negative Δr indicates stronger FA–GLN coupling in Low glycolysis. Glycerophospholipid and sphingolipid families show significantly lower coupling in High versus Low glycolysis. **Abbreviations:** Δr, difference in meta-correlation; q, FDR-adjusted p-value.

Table 4. Family-level differences in fatty acid–glutamine associations by glycolysis state.

Shown are Fisher-z meta-correlation differences (Δr, High–Low) for fatty acid (FA) families with two-sided P values and FDR-adjusted q values. Negative Δr indicates stronger FA–GLN coupling in glycolysis-low tumors; positive Δr indicates stronger coupling in glycolysis-high tumors. Family definitions/mappings are provided in S2 Table. FA family Δr_meta (High–Low).

FA family	Δr_meta (High–Low)	P value	FDR (q)	Interpretation
Sphingolipid	−0.12	0.0019	0.019	Lower in high (stronger in low); **significant**
Glycerophospholipid	−0.06	0.0041	0.021	Lower in high (stronger in low); **significant**

FA family	Δr_meta (High–Low)	P value	FDR (q)	Interpretation
FA biosynthesis/elongation	−0.08	0.048	0.161	Lower in high; nominal only
FAO β-oxidation	0.10	0.173	0.434	Higher in high; not significant
Lipid transport	0.09	0.457	0.761	Higher in high; not significant
TAG storage/lipolysis	−0.04	0.609	0.761	Lower in high; not significant
Unsaturated FA	−0.03	0.561	0.761	Lower in high; not significant
FAO carnitine shuttle	0.00	0.963	0.984	No difference
Lipid regulatory	0.00	0.984	0.984	No difference
Other FA	−0.02	0.594	0.761	Lower in high; not significant

Abbreviations: FA, fatty acid; GLN, glutamine; FAO, fatty acid oxidation; TAG, triacylglycerol; FDR, false discovery rate; q, FDR-adjusted P value.

Survival analysis stratified by glycolysis state

Cox models were applied at enzyme-class and family levels (Fig 5; Table 5,6). At the class level, LCFA activity was protective in glycolysis-high tumors (HR = 0.85, 95% CI 0.79–0.91, p = 1.0×10□□), borderline protective in glycolysis-medium tumors (HR = 0.93, 95% CI 0.86–1.01, p = 0.080), and not associated with survival in glycolysis-low tumors (HR = 0.99, 95% CI 0.93–1.06, p = 0.814). In glycolysis-low tumors, MCFA showed a borderline protective trend (HR = 0.89, 95% CI 0.78–1.02, p = 0.100). VLCFA trended toward higher hazard in glycolysis-medium tumors (HR = 1.10, 95% CI 0.98–1.23, p = 0.094). At the family level, in glycolysis-high tumors glycerophospholipid activity was associated with higher hazard (HR = 1.57, 95% CI 1.06–2.34, p = 0.025), whereas lipid transport (HR = 0.50, 95% CI 0.31–0.82, p = 0.006) and FAO carnitine shuttle (HR = 0.54, 95% CI 0.36–0.81, p = 0.003) were protective. In glycolysis-low tumors, lipid transport was also protective (HR= 0.64, 95% CI 0.42–0.99, p = 0.045). No families reached significance in the medium-glycolysis group.

Fig 5. Survival associations of FA metabolism by family and chain length, stratified by glycolysis. Hazard ratios (HRs) for overall survival with 95% confidence intervals are shown (per 1-SD increase in activity), with models adjusted for age, sex, and tumor stage. (A) Top FA families, colors indicate glycolysis state (Low = blue, Medium = orange, High = red). (B) Enzyme classes (MCFA = blue, LCFA = orange, VLCFA = green).Abbreviations: MCFA, medium-chain fatty acid; LCFA, long-chain fatty acid; VLCFA, very-long-chain fatty acid. **Abbreviations**: MCFA, medium chain fatty acid; LCFA, long chain fatty acid; VLCFA, very long chain fatty acid.

Table 5. Family-level Cox proportional hazards models stratified by glycolysis state.

Hazard ratios (HRs) are per 1-SD increase in ssGSEA-derived family activity and are adjusted for age, sex, and AJCC stage. P values are nominal (no FDR applied to survival models).

FA family	Low glycolysis HR (95% CI)	P value	Medium glycolysis HR (95% CI)	P value	High glycolysis HR (95% CI)	P value
Glycerophospholipid	0.98 (0.70–1.37)	0.917	1.10 (0.75–1.61)	0.612	1.57 (1.06–2.34)	0.025
Sphingolipid	1.09 (0.79–1.49)	0.592	1.05 (0.74–1.49)	0.778	1.22 (0.85–1.74)	0.274
Unsaturated FA	0.95 (0.70–1.29)	0.747	0.97 (0.68–1.39)	0.874	1.05 (0.73–1.52)	0.780
Lipid regulatory	1.02 (0.73–1.44)	0.896	1.01 (0.70–1.45)	0.952	0.99 (0.69–1.42)	0.970
Other FA	0.91 (0.67–1.25)	0.576	0.96 (0.66–1.39)	0.826	1.08 (0.74–1.57)	0.706
FA biosynthesis/elongation	0.94 (0.67–1.32)	0.721	1.02 (0.70–1.50)	0.916	0.97 (0.67–1.41)	0.885
FAO β-oxidation	0.92 (0.66–1.28)	0.618	0.99 (0.68–1.44)	0.962	1.05 (0.73–1.52)	0.784
TAG storage/lipolysis	1.00 (0.71–1.40)	0.990	1.03 (0.71–1.50)	0.876	0.97 (0.67–1.40)	0.856
Lipid transport	0.64 (0.42–0.99)	0.045	0.91 (0.61–1.37)	0.661	0.50 (0.31–0.82)	0.006
FAO carnitine shuttle	0.70 (0.49–1.01)	0.057	0.95 (0.66–1.38)	0.794	0.54 (0.36–0.81)	0.003

Abbreviations: FA, fatty acid; ssGSEA, single-sample gene set variation analysis; FAO, fatty acid oxidation; TAG, triacylglycerol; HR, hazard ratio; CI, confidence interval; SD, standard deviation.

Table 6. Class-level Cox proportional hazards models stratified by glycolysis state.

Hazard ratios (HRs) are per 1-SD increase in class activity (MCFA, LCFA, VLCFA) and are adjusted for age, sex, and AJCC stage. P values are nominal (no FDR applied).

FA class	Low glycolysis HR (95% CI)	P value	Medium glycolysis HR (95% CI)	P value	High glycolysis HR (95% CI)	P value	Interpretation
MCFA	0.89 (0.78–1.02)	0.100	1.04 (0.89–1.21)	0.643	0.95 (0.82–1.10)	0.494	Borderline protective in low; NS otherwise
LCFA	0.99 (0.93–1.06)	0.814	0.93 (0.86–1.01)	0.080	0.85 (0.79–0.91)	1.0×10□□	Protective in high; borderline protective in medium; NS in low
VLCFA	0.99 (0.90–1.08)	0.798	1.10 (0.98–1.23)	0.094	0.94 (0.85–1.03)	0.189	Borderline risk in medium; NS otherwise

Abbreviations: FA, fatty acid; MCFA, medium-chain fatty acid; LCFA, long-chain fatty acid; VLCFA, very-long-chain fatty acid; HR, hazard ratio; CI, confidence interval; SD, standard deviation; NS, not significant.

Supplementary predictive modeling

Permutation-based Elastic Net regression did not yield predictive performance beyond chance (Supplementary Fig S1, Supplementary Data S1, Supplementary Table S1): observed R^2 values did not differ significantly from the permutation-derived null distribution (1,000 permutations).

Supplementary metabolite-inference validation of FA–GLN coordination

Metabolite activities inferred from transcriptomic data were evaluated across the 173 PDAC tumors in the GENIE cohort (Supplementary Fig. S3 and Supplementary Fig. S4; Supplementary Table S3; Supplementary Table S5; Supplementary Data S5). Thirteen metabolites representing glutamine

metabolism (GLN, GLU, αKG), tricarboxylic acid (TCA) cycle intermediates (CITRATE, SUCCINATE, FUMARATE, MALATE), pyruvate–lactate exchange (PYRUVATE, LACTATE), fatty-acid oxidation (short/medium and long chain acyl-carnitines), very long chain fatty acid elongation (VLCFA_ELONG), and cellular redox buffering (GSH/GSSG) were analyzed. Unsupervised clustering of the resulting 13 × 173 activity matrix identified three metabolite-defined tumor states (Oxidative GLN-Driven, Hybrid FAO–TCA, Glycolytic FAO-Low), consistent with the dominant signatures illustrated in Supplementary Fig. S3 and Supplementary Fig. S4. A significant association was observed between glycolysis strata and the three metabolite-defined states ($\chi^2 = 14.54$, df = 4, $p = 0.0059$; Cramér's V = 0.21), indicating that coordinated metabolite phenotypes were modulated by glycolytic background. Differences in individual metabolite activities across the three states were examined using one-way ANOVA and the Kruskal–Wallis test. After Benjamini–Hochberg correction, statistically significant differences (FDR < 0.05) were detected for all 13 metabolites across the three states (Supplementary Table S4). The largest effects were observed for TCA-cycle intermediates (MALATE, SUCCINATE, FUMARATE), αKG, long chain acyl-carnitines, and VLCFA elongation, whereas PYRUVATE exhibited the weakest but still significant difference. Alignment between metabolite-defined states and transcriptomic FA–GLN coordination was examined. Low-glycolysis tumors, which previously showed the strongest GLN–TCA–lipid coordination transcriptomically, corresponded to the Oxidative GLN-Driven State. Medium-glycolysis tumors, which showed the strongest VLCFA–GLN coupling, corresponded to the Hybrid FAO–TCA State, characterized by elevated long-chain acyl-carnitines and increased FAO. High-glycolysis tumors, which demonstrated weak FA–GLN coordination, corresponded to the Glycolytic FAO-Low State, consistent with reduced acyl-carnitines and diminished oxidative metabolism. Together, these findings demonstrated that the FA–GLN metabolic hierarchy identified in pathway-level transcriptomic analyses was preserved when evaluated through metabolite-inference modeling and remained stratified by glycolytic background.

Discussion

This study profiled fatty acid (FA) metabolism in PDAC patient tumors with attention to chain length, lipid families, and glycolytic state. Three consistent findings emerged. First, FA–GLN coupling was strongly context-dependent: in glycolysis-low tumors, sphingolipid and glycerophospholipid pathways correlated most strongly with GLN activity, whereas aminoacyl-tRNA pathways dominated in glycolysis-medium tumors, and few FA pathways correlated with GLN in glycolysis-high tumors. Second, enzyme-class meta-analysis indicated that VLCFA enzymes showed the tightest positive association with GLN in medium-glycolysis tumors, while MCFA enzymes weakened or inverted their association in glycolysis-high tumors. Third, family-level correlations for glycerophospholipids and sphingolipids were significantly lower in high versus low glycolysis tumors, suggesting a decoupling of lipid remodeling from GLN metabolism as glycolytic dependence increases.

Clinical associations paralleled these patterns. At the class level, LCFA activity was protective in glycolysis-high tumors, borderline protective in glycolysis-medium tumors, and not associated with outcome in glycolysis-low tumors. At the family level, glycerophospholipid activity associated with higher hazard in glycolysis-high tumors, whereas lipid transport and FAO carnitine-shuttle activity were protective in both high and low glycolysis states. Together, these results argue that FA biology in PDAC is heterogeneous and that prognostic effects depend on both chain length and glycolytic context.

These observations provide a patient-based complement to preclinical work showing that altering nutrient availability (for example, ketogenic-diet conditions) modulates responsiveness to GLN-pathway inhibition. The present data refine that concept by indicating that not all FA classes behave similarly across glycolytic states: membrane-focused families (glycerophospholipids, sphingolipids) appear preferentially coupled to GLN in glycolysis-low tumors, whereas in glycolysis-high tumors the same families lose this coupling and glycerophospholipid activity associates with worse survival. One interpretation is that when glycolysis is low, GLN anaplerosis and lipid remodeling are coordinated to sustain biomass and signaling; as glycolysis rises, carbohydrate-derived carbons may partially substitute

for GLN-linked lipid programs, weakening coupling and shifting the prognostic role of specific FA families. The stronger GLN association for VLCFA enzymes in medium-glycolysis tumors may reflect increased demands for membrane elongation/desaturation or peroxisomal contributions during intermediate metabolic states. These mechanisms remain hypotheses that require flux-level validation.

Additionally, Elastic-Net analysis confirmed that FA pathways, despite their associations with GLN activity, do not provide strong predictive power for GLN levels, indicating that these relationships reflect coordinated metabolic patterns rather than direct predictiveness. In medium-glycolysis tumors, the prominence of aminoacyl-tRNA pathways is interpreted as reflecting GLN-dependent biosynthetic activity rather than FA-specific coordination.

To evaluate whether these transcriptomically derived FA–GLN coordination patterns reflected broader metabolic programs, a supplementary metabolite-inference analysis was performed. Three metabolite-defined states were identified and were shown to differ significantly across all evaluated metabolites. These states paralleled the FA–GLN hierarchy: the Oxidative GLN-Driven State corresponded to low-glycolysis tumors, the Hybrid FAO–TCA State corresponded to medium-glycolysis tumors, and the Glycolytic FAO-Low State corresponded to high-glycolysis tumors. The preservation of these relationships indicated that the FA–GLN metabolic architecture observed in pathway-level transcriptomic analyses reflected broader, coordinated metabolic programs when evaluated from a metabolite-inference perspective.

Limitations of this study include reliance on bulk RNA-seq and enrichment-based pathway activity (which do not measure flux or resolve cell-type contributions) and reduced power within glycolysis strata for survival analyses. Gene-set definitions of FA “families” may not capture all biochemical specificities, and results may be sensitive to curation choices. The study is observational and cross-sectional, so causal inferences cannot be drawn. Finally, predictive modeling with Elastic Net did not outperform permutation

nulls, indicating that while associations are robust, GLN activity is not readily predicted from FA pathways alone within strata.

Implications and next steps. Stratifying PDAC by glycolytic state may be necessary when evaluating FA or GLN-directed interventions and when interpreting dietary manipulations that shift circulating FA composition. Prospective studies should (i) combine tumor glycolysis readouts (for example, transcriptomic scores or FDG-PET) with lipidomics and stable-isotope tracing, (ii) validate chain length–specific effects in controlled perturbations (MCFA versus LCFA availability) with and without GLN pathway inhibitors, and (iii) use single-cell and spatial approaches to resolve tumor–stroma contributions to FA and GLN programs.

Conclusion

FA metabolism in PDAC is not uniform; its associations with GLN metabolism and with patient outcomes depend on both chain length and glycolytic state. Glycerophospholipid and sphingolipid families show the strongest link to GLN in glycolysis-low tumors but are decoupled in glycolysis-high tumors, where glycerophospholipid activity associates with poorer survival. LCFA activity is protective in glycolysis-high tumors and shows a borderline protective trend in medium glycolysis. These glycolysis stratified patterns define conditional metabolic vulnerabilities and provide a rationale to incorporate tumor glycolytic state and FA class composition when designing GLN-targeted or diet-modulated therapeutic strategies.

Data Availability. All supplementary figures, tables, and source data used in this study are publicly available at Zenodo under the following DOI: https://doi.org/10.5281/zenodo.17688982. All code used for analysis is available upon request or can be provided in a separate repository if required for review. No restrictions apply to data access.

References

1. Siegel RL, Miller KD, Fuchs HE, Jemal A. Cancer statistics, 2024. CA Cancer J Clin. 2024;74(1):17–48.
2. Rahib L, Smith BD, Aizenberg R, Rosenzweig AB, Fleshman JM, Matrisian LM. Projecting cancer incidence and deaths to 2030: the unexpected burden of thyroid, liver, and pancreas cancers. Cancer Res. 2014;74(11):2913–21.
3. Pavlova NN, Thompson CB. The emerging hallmarks of cancer metabolism. Cell Metab. 2016;23(1):27–47.
4. Vander Heiden MG, DeBerardinis RJ. Understanding the intersections between metabolism and cancer biology. Cell. 2017;168(4):657–69.
5. Hanahan D, Weinberg RA. Hallmarks of cancer: the next generation. Cell. 2011;144(5):646–74.
6. Kamphorst JJ, Nofal M, Commisso C, Hackett SR, Lu W, Grabocka E, et al. Human pancreatic tumors are nutrient poor and tumor cells actively scavenge extracellular protein. Cancer Res. 2015;75(3):544–53.
7. Ying H, Kimmelman AC, Lyssiotis CA, Hua S, Chu GC, Fletcher-Sananikone E, et al. Oncogenic KRAS maintains pancreatic tumors through regulation of anabolic glucose metabolism. Cell. 2012;149(3):656–70.
8. Bailey P, Chang DK, Nones K, Johns AL, Patch AM, Gingras MC, et al. Genomic analyses identify molecular subtypes of pancreatic cancer. Nature. 2016;531(7592):47–52.
9. Altman BJ, Stine ZE, Dang CV. From Krebs to clinic: glutamine metabolism to cancer therapy. Nat Rev Cancer. 2016;16(10):619–34.
10. Son J, Lyssiotis CA, Ying H, Wang X, Hua S, Ligorio M, et al. Glutamine supports pancreatic cancer growth through a KRAS-regulated metabolic pathway. Nature. 2013;496(7443):101–5.

11. Hensley CT, Wasti AT, DeBerardinis RJ. Glutamine and cancer: cell biology, physiology, and clinical opportunities. J Clin Invest. 2013;123(9):3678–84.
12. Encarnación-Rosado J, Chen HC, Tu J, Taniguchi K, Guo Q, Cui Y, et al. Pharmacological inhibition of glutamine metabolism by DON induces metabolic crisis in PDAC. Cancer Discov. 2024;14(5):1123–35.
13. Sousa CM, Biancur DE, Wang X, Halbrook CJ, Sherman MH, Zhang L, et al. Pancreatic stellate cells support tumor metabolism through autophagic alanine secretion. Nature. 2016;536(7617):479–83.
14. Röhrig F, Schulze A. The multifaceted roles of fatty acid synthesis in cancer. Nat Rev Cancer. 2016;16(11):732–49.
15. Koundouros N, Poulogiannis G. Reprogramming of fatty acid metabolism in cancer. Br J Cancer. 2020;122(1):4–22.
16. Schug ZT, Vande Voorde J, Gottlieb E. The metabolic fate of acetate in cancer. Nat Rev Cancer. 2016;16(11):708–17.
17. Nagarajan SR, Butler LM, Hoy AJ. The diversity and breadth of cancer cell fatty acid metabolism. Cancer Metab. 2021; 9:2.
18. Hajihassani O, Zarei M, Roichman A, Sadeh R, Eilam R, Wainberg Z, et al. A ketogenic diet sensitizes pancreatic cancer to inhibition of glutamine metabolism. bioRxiv. 2024. doi:10.1101/2024.07.19.604377.
19. Jin J, Byun J-K, Choi Y-K, Park K-G. Targeting glutamine metabolism as a therapeutic strategy for cancer. Exp Mol Med. 2023; 55:706–15.
20. AACR Project GENIE Consortium. AACR Project GENIE: powering precision medicine through an international consortium. Cancer Discov. 2017;7(8):818–31.
21. Kanehisa M, Furumichi M, Sato Y, Kawashima M, Ishiguro-Watanabe M. KEGG for taxonomy-based analysis of pathways and genomes. Nucleic Acids Res. 2023;51(D1): D587–92.

22. Jassal B, Matthews L, Viteri G, Gong C, Lorente P, Fabregat A, et al. The Reactome pathway knowledgebase. Nucleic Acids Res. 2020;48(D1): D498–503.
23. Kutmon M, Riutta A, Nunes N, Hanspers K, Willighagen EL, Bohler A, et al. WikiPathways: capturing the full diversity of pathway knowledge. Nucleic Acids Res. 2016;44(D1): D661–7.
24. Liberzon A, Birger C, Thorvaldsdóttir H, Ghandi M, Mesirov JP, Tamayo P. The MSigDB hallmark gene-set collection. Cell Syst. 2015;1(6):417–25.
25. Hänzelmann S, Castelo R, Guinney J. GSVA: gene set variation analysis for microarray and RNA-seq data. BMC Bioinformatics. 2013; 14:7.
26. Benjamini Y, Hochberg Y. Controlling the false discovery rate: a practical and powerful approach to multiple testing. J R Stat Soc B. 1995;57(1):289–300.
27. Cox DR. Regression models and life-tables. J R Stat Soc B. 1972;34(2):187–220.
28. Zou H, Hastie T. Regularization and variable selection via the elastic net. J R Stat Soc B. 2005;67(2):301–20.
29. Efron B, Tibshirani RJ. An Introduction to the Bootstrap. Boca Raton: Chapman & Hall/CRC; 1994.
30. Harris CR, Millman KJ, van der Walt SJ, Gommers R, Virtanen P, Cournapeau D, et al. Array programming with NumPy. Nature. 2020;585(7825):357–62.
31. McKinney W. Data structures for statistical computing in Python. In: van der Walt S, Millman J, editors. Proceedings of the 9th Python in Science Conference. 2010. p. 51–56.
32. Pedregosa F, Varoquaux G, Gramfort A, Michel V, Thirion B, Grisel O, et al. Scikit-learn: Machine learning in Python. J Mach Learn Res. 2011; 12:2825–30.
33. Hunter JD. Matplotlib: A 2D graphics environment. Comput Sci Eng. 2007;9(3):90–5.

Supporting information

S1 Fig. Elastic-Net out-of-fold predictions for GLN activity by glycolysis grouping.

Scatter of predicted versus observed glutamine (GLN) pathway activity with y = x reference (dashed). Panels: All (locked model), High glycolysis, Low glycolysis, High glycolysis subset (extreme samples), and Low glycolysis subset (extreme samples). Each point is a patient sample (n = All 172; High glycolysis 86; Low glycolysis 86; High glycolysis subset 57; Low glycolysis subset 57). Out-of-fold performance per panel: All $R^2 = 0.247$, RMSE = 0.0197; High glycolysis $R^2 = 0.283$, RMSE = 0.0204; Low glycolysis $R^2 = 0.033$, RMSE = 0.0209; High glycolysis subset $R^2 = –0.030$, RMSE = 0.0231; Low glycolysis subset $R^2 = –0.073$, RMSE = 0.0236. The 'All' panel shows OOF predictions from a single model trained/tuned on the full cohort and then fixed; other panels show models trained/tuned within the indicated subsets. Abbreviations: GLN, glutamine; RMSE, root mean squared error.

S1 Table. Cross-validated performance metrics by grouping.

Compact summary of Elastic-Net out-of-fold performance. Columns: Group, R^2_OOF, RMSE_OOF. Reported values: All $R^2 = 0.247$, RMSE = 0.0197; High glycolysis $R^2 = 0.283$, RMSE = 0.0204; Low glycolysis $R^2 = 0.033$, RMSE = 0.0209; High glycolysis subset $R^2 = –0.030$, RMSE = 0.0231; Low glycolysis subset $R^2 = –0.073$, RMSE = 0.0236.

S1 Data. Out-of-fold predictions by grouping.

Columns: group (All, High glycolysis, Low glycolysis, High glycolysis subset, Low glycolysis subset), observed GLN activity, predicted GLN activity, and sample_id.

S2 Table. Fatty acid family definitions and pathway membership (mapping).

Curated mapping of fatty acid (FA) pathways/enzymes to functional families (glycerophospholipid, sphingolipid, FA biosynthesis/elongation, FAO β-oxidation, lipid transport, TAG storage/lipolysis, unsaturated FA, FAO carnitine shuttle, lipid regulatory). Columns: Pathway name, Family. Used for gene-set scoring and family-level analyses.

S3 Fig. Principal component analysis (PCA) of inferred metabolite activities. PCA plot of z-scored inferred metabolite activity profiles across GENIE-PDAC tumors. Each point represents one patient sample (n=173). Samples are colored by the three metabolite-defined metabolic phenotypes (Oxidative GLN-Driven, Hybrid FAO–TCA, Glycolytic FAO-Low). PC1 and PC2 visually separate metabolic states, demonstrating coordinated variation in GLN/TCA/FAO-linked metabolite activities. Loadings correspond to the 13 inferred metabolites. Abbreviations: PCA, principal component analysis; GLN, glutamine; FAO, fatty-acid oxidation; TCA, tricarboxylic acid.

S3 Table. Inferred metabolite activity scores (raw and z-scored).

Matrix of inferred metabolite activities derived from the curated metabolite–gene mapping. Columns include sample ID, raw weighted activity scores for each metabolite, and corresponding z-scored values. These scores were used forPCA, clustering, and downstream metabolic state assignment. Columns: sample_id, metabolite_raw_score (×13), metabolite_zscore (×13).

S4 Fig. Heatmap of mean metabolite activities across metabolite-defined metabolic phenotypes. Heatmap depicting mean z-scored activities for each metabolite within the three metabolic phenotypes. Rows represent metabolites (n=13) and columns represent metabolic states. Color intensity reflects standardized activity, showing elevated GLN/αKG/TCA/redox signatures in the Oxidative GLN-Driven state, mixed elevation in the Hybrid FAO–TCA state, and reduced FAO/acyl-carnitine activity in the Glycolytic FAO-Low state. Abbreviations: GLN, glutamine; αKG, alpha-ketoglutarate; FAO, fatty-acid oxidation; TCA, tricarboxylic acid cycle.

S4 Table. Statistical comparisons of inferred metabolite activities across metabolic phenotypes. One-way ANOVA and Kruskal–Wallis (KW) p-values for each inferred metabolite across the three metabolic phenotypes (n=173 samples). For each metabolite, the F-statistic, KW-statistic, unadjusted p-

values, and FDR- adjusted p-values are reported. Several metabolites show significant differences across states (FDR < 0.05). Columns: metabolite, ANOVA_F, ANOVA_p, KW_H, KW_p, FDR_p.

S5 Table. Curated metabolite–gene mapping with directionality assignments.

Mapping of each metabolite to associated enzymes and transporters with +1/–1 directionality weights based on biochemical relationships. This table defines the weighted gene contributions used to compute metabolite activity scores. Columns: metabolite, gene, direction (+1 or –1).

S5 Data. Final metabolic state labels for all PDAC samples.

Sample-level assignments to one of the three metabolite-defined metabolic phenotypes (Oxidative GLN-Driven, Hybrid FAO–TCA, Glycolytic FAO-Low). Columns: sample_id, metabolic_state.

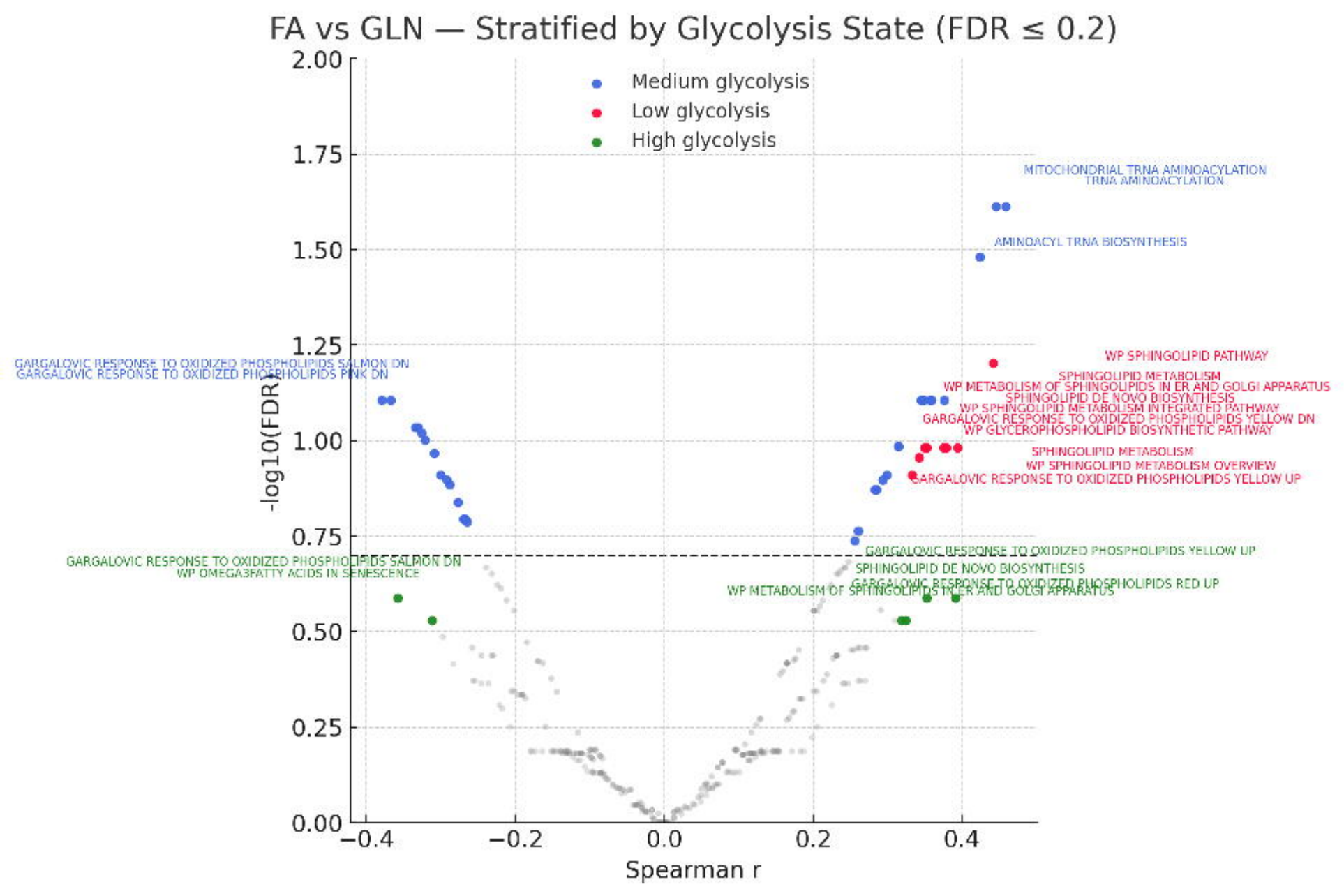
FA vs GLN — Stratified by Glycolysis State (FDR ≤ 0.2)
Medium glycolysis
Low glycolysis
High glycolysis
MITOCHONDRIAL TRNA AMINOACYLATION
TRNA AMINOACYLATION
AMINOACYL TRNA BIOSYNTHESIS
WP SPHINGOLIPID PATHWAY
SPHINGOLIPID METABOLISM
WP METABOLISM OF SPHINGOLIPIDS IN ER AND GOLGI APPARATUS
SPHINGOLIPID DE NOVO BIOSYNTHESIS
WP SPHINGOLIPID METABOLISM INTEGRATED PATHWAY
GARGALOVIC RESPONSE TO OXIDIZED PHOSPHOLIPIDS YELLOW DN
WP GLYCEROPHOSPHOLIPID BIOSYNTHETIC PATHWAY
SPHINGOLIPID METABOLISM
WP SPHINGOLIPID METABOLISM OVERVIEW
GARGALOVIC RESPONSE TO OXIDIZED PHOSPHOLIPIDS YELLOW UP
GARGALOVIC RESPONSE TO OXIDIZED PHOSPHOLIPIDS SALMON DN
GARGALOVIC RESPONSE TO OXIDIZED PHOSPHOLIPIDS PINK DN
GARGALOVIC RESPONSE TO OXIDIZED PHOSPHOLIPIDS YELLOW UP
SPHINGOLIPID DE NOVO BIOSYNTHESIS
GARGALOVIC RESPONSE TO OXIDIZED PHOSPHOLIPIDS RED UP
WP METABOLISM OF SPHINGOLIPIDS IN ER AND GOLGI APPARATUS
GARGALOVIC RESPONSE TO OXIDIZED PHOSPHOLIPIDS SALMON DN
WP OMEGA3FATTY ACIDS IN SENESCENCE
-log10(FDR)
Spearman r
2.00
1.75
1.50
1.25
1.00
0.75
0.50
0.25
0.00
−0.4
−0.2
0.0
0.2
0.4

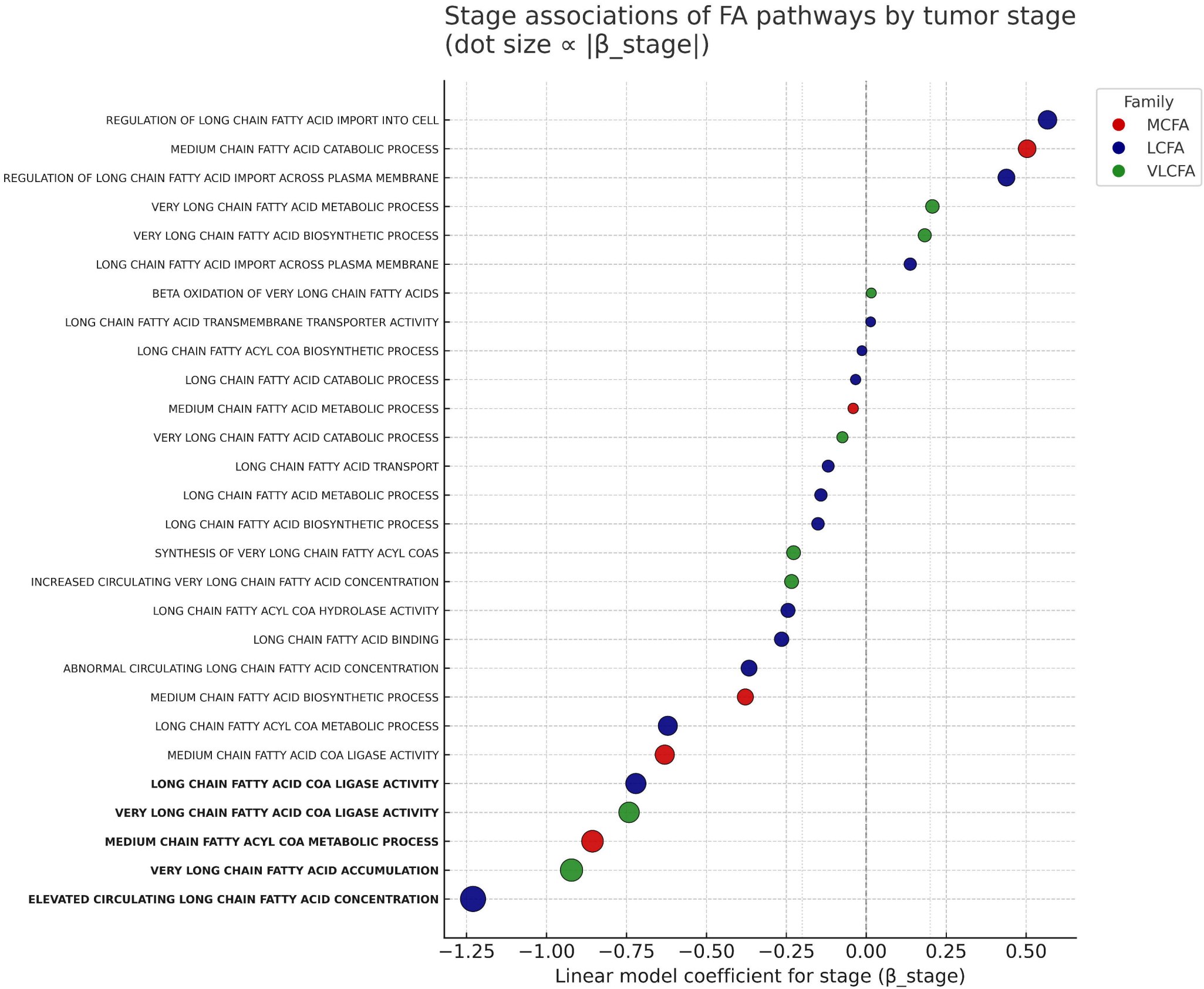
Stage associations of FA pathways by tumor stage
(dot size ∝ |β_stage|)
REGULATION OF LONG CHAIN FATTY ACID IMPORT INTO CELL
MEDIUM CHAIN FATTY ACID CATABOLIC PROCESS
REGULATION OF LONG CHAIN FATTY ACID IMPORT ACROSS PLASMA MEMBRANE
VERY LONG CHAIN FATTY ACID METABOLIC PROCESS
VERY LONG CHAIN FATTY ACID BIOSYNTHETIC PROCESS
LONG CHAIN FATTY ACID IMPORT ACROSS PLASMA MEMBRANE
BETA OXIDATION OF VERY LONG CHAIN FATTY ACIDS
LONG CHAIN FATTY ACID TRANSMEMBRANE TRANSPORTER ACTIVITY
LONG CHAIN FATTY ACYL COA BIOSYNTHETIC PROCESS
LONG CHAIN FATTY ACID CATABOLIC PROCESS
MEDIUM CHAIN FATTY ACID METABOLIC PROCESS
VERY LONG CHAIN FATTY ACID CATABOLIC PROCESS
LONG CHAIN FATTY ACID TRANSPORT
LONG CHAIN FATTY ACID METABOLIC PROCESS
LONG CHAIN FATTY ACID BIOSYNTHETIC PROCESS
SYNTHESIS OF VERY LONG CHAIN FATTY ACYL COAS
INCREASED CIRCULATING VERY LONG CHAIN FATTY ACID CONCENTRATION
LONG CHAIN FATTY ACYL COA HYDROLASE ACTIVITY
LONG CHAIN FATTY ACID BINDING
ABNORMAL CIRCULATING LONG CHAIN FATTY ACID CONCENTRATION
MEDIUM CHAIN FATTY ACID BIOSYNTHETIC PROCESS
LONG CHAIN FATTY ACYL COA METABOLIC PROCESS
MEDIUM CHAIN FATTY ACID COA LIGASE ACTIVITY
LONG CHAIN FATTY ACID COA LIGASE ACTIVITY
VERY LONG CHAIN FATTY ACID COA LIGASE ACTIVITY
MEDIUM CHAIN FATTY ACYL COA METABOLIC PROCESS
VERY LONG CHAIN FATTY ACID ACCUMULATION
ELEVATED CIRCULATING LONG CHAIN FATTY ACID CONCENTRATION
−1.25
−1.00
−0.75
−0.50
−0.25
0.00
0.25
0.50
Linear model coefficient for stage (β_stage)
Family
MCFA
LCFA
VLCFA

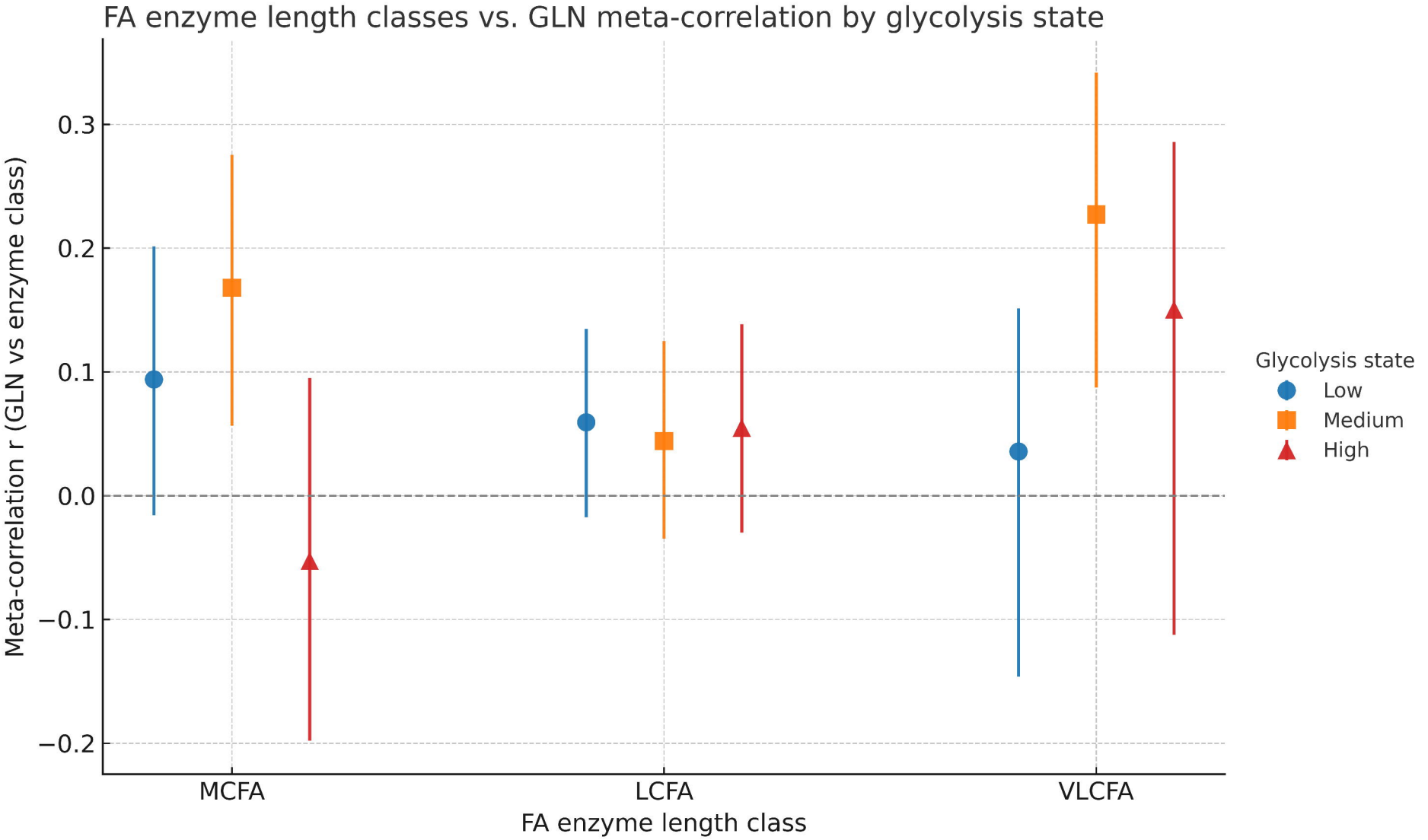
FA enzyme length classes vs. GLN meta-correlation by glycolysis state
Meta-correlation r (GLN vs enzyme class)
0.3
0.2
0.1
0.0
−0.1
−0.2
MCFA
LCFA
VLCFA
FA enzyme length class
Glycolysis state
Low
Medium
High

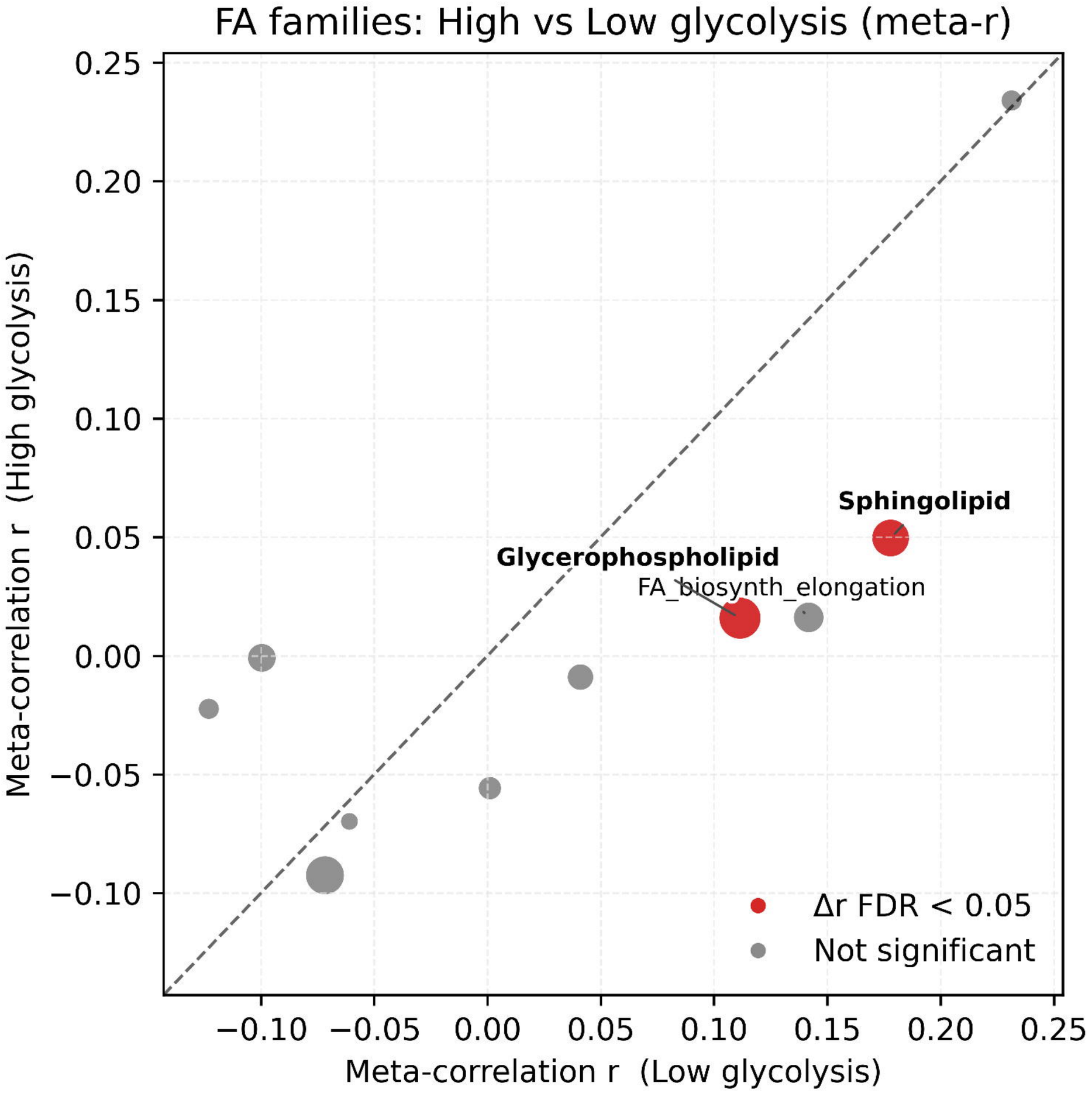
FA families: High vs Low glycolysis (meta-r)
Sphingolipid
Glycerophospholipid
FA_biosynth_elongation
Δr FDR < 0.05
Not significant
Meta-correlation r (High glycolysis)
Meta-correlation r (Low glycolysis)
0.25
0.20
0.15
0.10
0.05
0.00
−0.05
−0.10
−0.10
−0.05
0.00
0.05
0.10
0.15
0.20
0.25

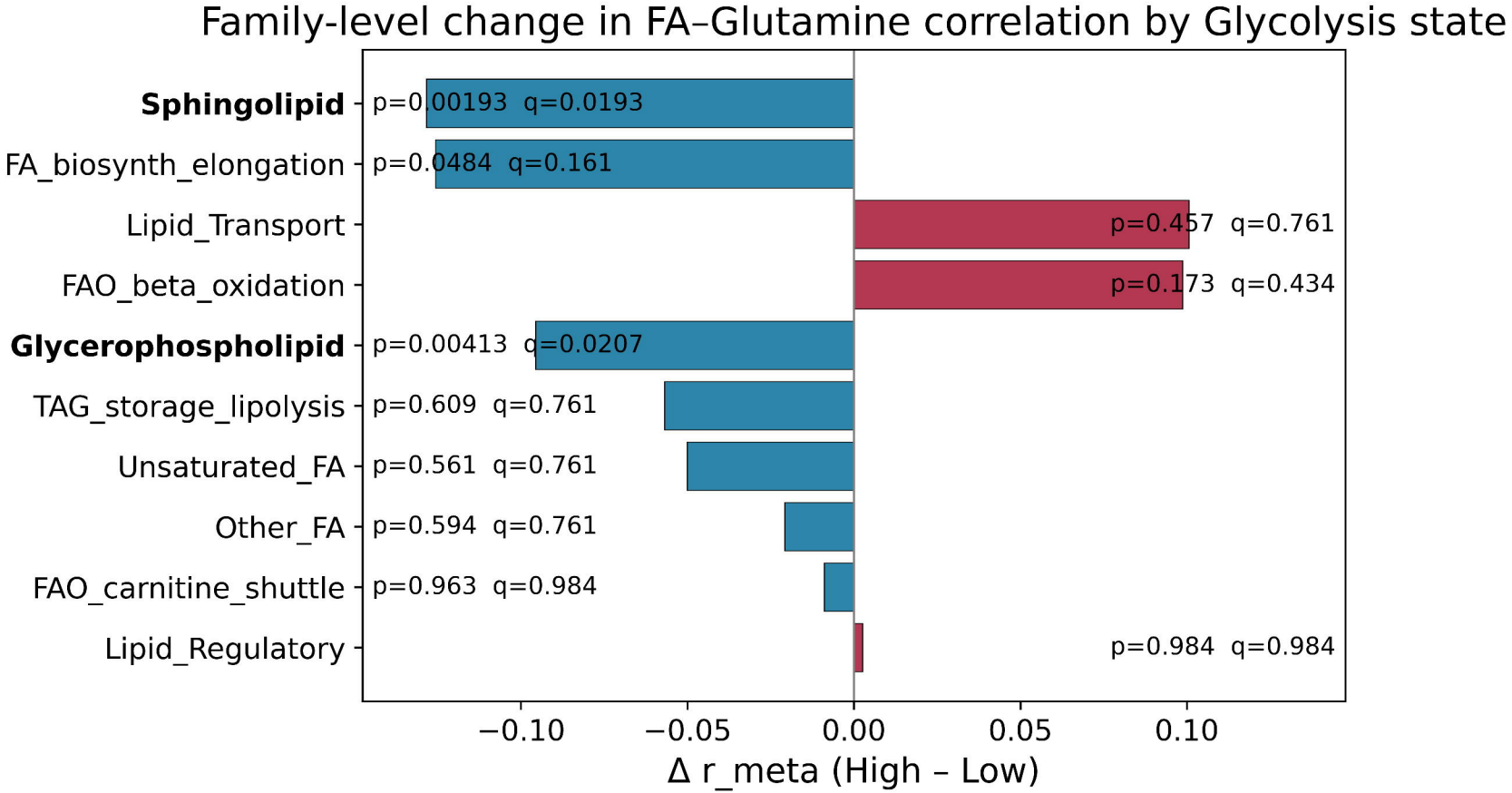
Family-level change in FA–Glutamine correlation by Glycolysis state
Sphingolipid
FA_biosynth_elongation
Lipid_Transport
FAO_beta_oxidation
Glycerophospholipid
TAG_storage_lipolysis
Unsaturated_FA
Other_FA
FAO_carnitine_shuttle
Lipid_Regulatory
p=0.00193 q=0.0193
p=0.0484 q=0.161
p=0.457 q=0.761
p=0.173 q=0.434
p=0.00413 q=0.0207
p=0.609 q=0.761
p=0.561 q=0.761
p=0.594 q=0.761
p=0.963 q=0.984
p=0.984 q=0.984
−0.10
−0.05
0.00
0.05
0.10
Δ r_meta (High – Low)

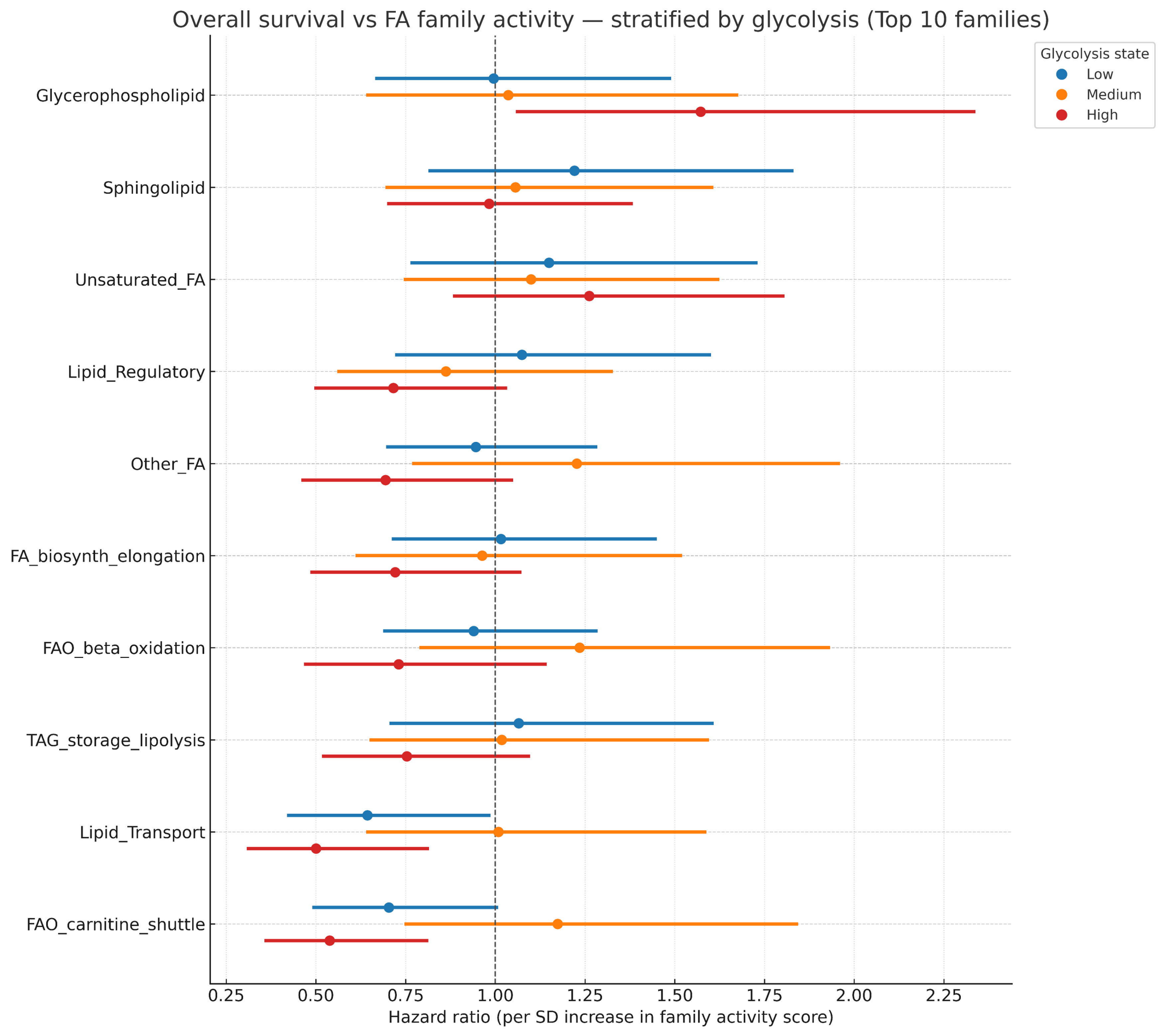
Overall survival vs FA family activity — stratified by glycolysis (Top 10 families)
Glycolysis state
Low
Medium
High
Glycerophospholipid
Sphingolipid
Unsaturated_FA
Lipid_Regulatory
Other_FA
FA_biosynth_elongation
FAO_beta_oxidation
TAG_storage_lipolysis
Lipid_Transport
FAO_carnitine_shuttle
0.25
0.50
0.75
1.00
1.25
1.50
1.75
2.00
2.25
Hazard ratio (per SD increase in family activity score)

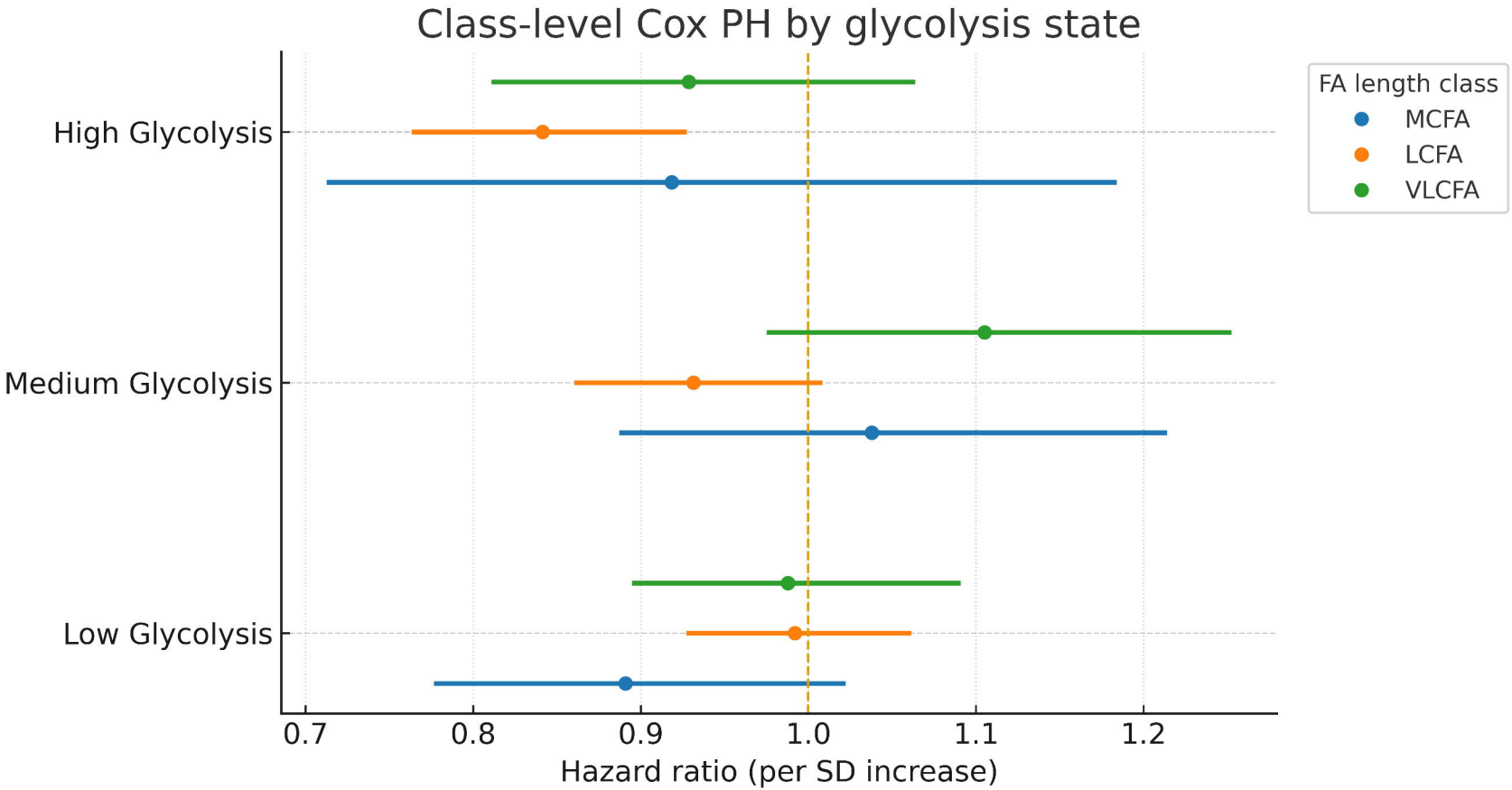
Class-level Cox PH by glycolysis state
High Glycolysis
Medium Glycolysis
Low Glycolysis
0.7
0.8
0.9
1.0
1.1
1.2
Hazard ratio (per SD increase)
FA length class
MCFA
LCFA
VLCFA